STAR Results from the RHIC Beam Energy Scan

Hui Wang for the STAR collaboration

RM 1-174, Building 510A, Brookhaven National Laboratory, Upton, NY, 11973

E-mail: `wanghui6@bnl.gov`

Abstract.

The collision of two gold nuclei at top RHIC energy ($\sqrt{s_{NN}}$=200 GeV) creates a new phase of matter, the quark-gluon plasma (QGP). The QGP exists at very high temperatures, T, and low baryo-chemical potentials, μ_B. Both lattice QCD and experimental data indicate this transition from hadronic matter to Quark Gluon Plasma is an analytical transition (cross-over). On the other hand, systems formed at larger values of the baryo-chemical potential may undergo a first-order transition. Thus there can be an end point of the first-order transition on the QCD phase diagram, the critical point.

To study the QCD phase boundary and search for the possible QCD critical point, RHIC launched a Beam Energy Scan Program. In 2010 and 2011, we collected data at $\sqrt{s_{NN}}$=7.7, 11.5, 19.6, 27, 39 and 62.4 GeV, which covers a wide range of baryon chemical potential from μ_B 420 to 40 MeV. In this article, we will report the latest results of the Beam Energy Scan Program from the STAR collaboration.

1. Introduction

Current results from RHIC and LHC indicate the existence of a deconfined Quark Gluon Plasma (QGP) phase at high energy in A+A collisions. One major challenge, however, is to understand the structure of the QCD phase diagram. If the temperature is high and μ_B is relatively small, both lattice QCD and experimental data indicate this transition from hadronic matter to Quark Gluon Plasma is an analytical transition (cross-over) [1], while some theoretical calculations predict that the transition at lower temperatures and high μ_B is a first order phase transition [2]. If a phase transition exists at higher μ_B, with a cross-over at $\mu_B = 0$, the phase transition would end in a critical point at finite μ_B. However, due to the difficulty of lattice QCD calculations at finite μ_B, accurate predictions of the critical point location are still lacking [3]. Therefore it falls to experiment to search for traces of the existence of the critical point of QCD.

To further explore the QCD phase diagram, a Beam Energy Scan (BES) proposal was made by the STAR Collaboration [4], which aims to search for the turn-off of QGP signatures, signals for first order phase transition and the critical point. The first phase of the BES program was started in 2010 with collisions recorded at $\sqrt{s_{NN}} = 7.7$, 11.5, 39 GeV and finished in 2011 with collisions at $\sqrt{s_{NN}}$=19.6 and 27 GeV. In this paper, a few selected results from the STAR BES program will be discussed.

2. Accessing the Phase Diagram

One important measurement related to the QCD Phase Diagram is the chemical freeze-out and kinetic freeze-out parameters from different collision energies and centralities. If we assume

thermodynamical equilibrium, a statistical thermal model (THERMUS)[5] can be used to determine the chemical freeze-out temperature T_{ch} and baryon chemical potential μ_B. At STAR, the THERMUS model was used to fit mid-rapidity particle ratios including yields of π, K, p, K^0_S, Λ and Ξ measured in Au+Au collisions at $\sqrt{s_{NN}}$= 7.7, 11.5, 39 and 200 GeV [6]. Figure 1 shows centrality and energy dependence of the extracted chemical freeze-out parameters using the Grand-Canonical Ensemble (GCE) approach of THERMUS, while the curves represent different parametrizations [7, 8]. A large μ_B range of 20 to 400 MeV is covered with the BES energies.
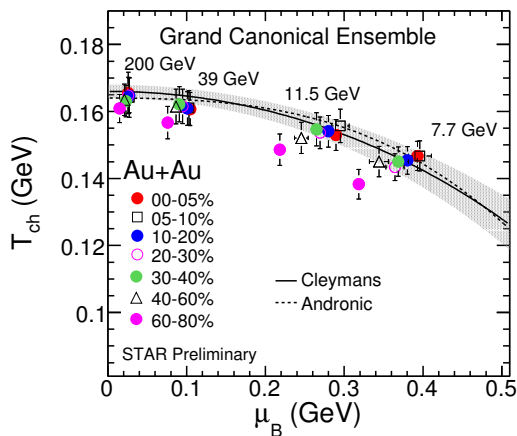
Figure 1. Centrality and energy dependence of the extracted chemical freeze-out parameters.
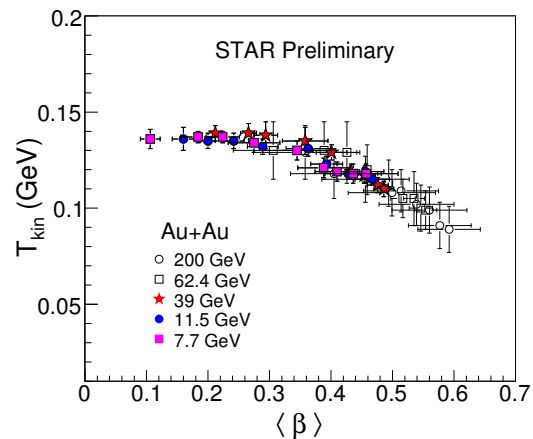
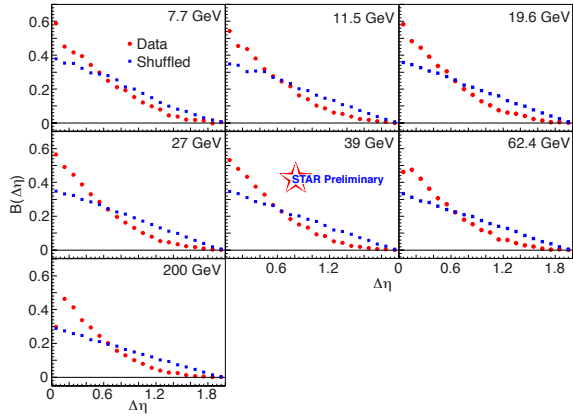**Figure 2.** Centrality and energy dependence of the extracted kinetic freeze-out parameters.

The kinetic freeze-out is the point where all elastic collisions among the particles stop. By doing the simultaneous fits of π, K, and p transverse momentum spectra to a blast-wave model, one can determine the kinetic freeze-out temperature T_{kin} and average flow velocity $\langle \beta \rangle$. Figure 2 shows the variation of T_{kin} as a function of $\langle \beta \rangle$ at $\sqrt{s_{NN}}$= 7.7, 11.5, 39, 62.4 and 200 GeV. The T_{kin} decreases with increasing collision centralities and energy, while the $\langle \beta \rangle$ increases with increasing collision centralities and energy.

3. Search for Turn-off of QGP Signatures
3.1. the Balance Function
The balance functions, which measure the correlation between the opposite sign charge pairs, are sensitive to the mechanisms of charge formation and the subsequent relative diffusion of the balancing charges [9]. Due to conservation laws like electric charge conservation, particles and their anti-particles are pair produced and correlated initially in coordinate space, if a delayed hadronization occurs, the lower temperature and less expansion and diffusion will result in a narrower charge balance function. It has been reported that the balance function for $\Delta\eta$ narrows at top RHIC energies [10]. Thus the balance function could be used to probe the evolution of the system hadronization time vs. energy and search for possible turn-off of QGP at lower energies.

Figure 3 shows the balance function in terms of $\Delta\eta$ for all charged particles. The most central events (0-5%) are shown for seven incident energies. The data in the figure are the balance function results from real data corrected by subtracting the balance function calculated using mixed events. We can see that, for all the energies shown here, the balance functions from data are narrower than the ones from shuffled events. To quantify the narrowing of balance function,

Figure 3. The balance function in terms of $\Delta\eta$ for all charged particles. Central events (0-5%) are shown here with $\sqrt{s_{NN}}$ from 7.7 to 200 GeV.
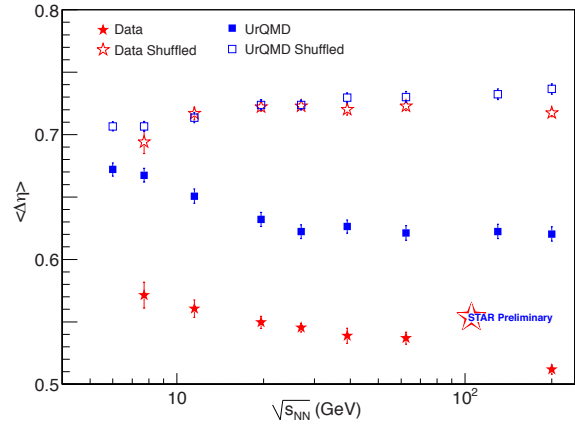
Figure 4. Energy dependence of the balance function width $\langle\Delta\eta\rangle$ for central Au+Au collisions (0-5%) compared with shuffled events. Both data and UrQMD calculations are shown here.

figure 4 shows the energy dependence of the balance function width for central Au+Au collisions. The data show a smooth decrease of $\langle\Delta\eta\rangle$ with increasing energy. UrQMD calculations predict a similar trend but over predict the observed results. Since the balance function is sensitive to the hadronization time and relative diffusion after hadronization, this decrease in balance function width could mean a longer lived QGP phase at higher energies. The UrQMD model is a hadronic model that does not have a deconfined phase transition and has little flow. This early hadronization time combined with strong interaction between final particles leads to a wider balance function in UrQMD. In the same figure, the shuffled events from both data and UrQMD show a wider balance function that slightly increases with increasing energy. Since the shuffled events represent the widest balance function within STAR's acceptance, the change of the balance function calculated using shuffled events is due to the slight changes in STAR's η acceptance with energy.

3.2. Elliptic Flow
Elliptic flow is the second harmonic coefficient of the Fourier expansion

$$\frac{dN}{d\phi} \propto 1 + 2\sum_{n\geq1} v_n \cos\left[n(\phi - \Psi)\right] \qquad (1)$$

where ϕ is the azimuthal angle of the particles and Ψ is the reconstructed event plane azimuthal angle. Elliptic flow is generated by the initial pressure gradient created by non-central heavy ion collisions. One major evidence that a deconfined quark gluon plasma is produced in Au+Au collisions at $\sqrt{s_{NN}} = 200$ GeV is the number-of-constituent quark (NCQ) scaling of v_2 versus transverse momentum p_T for hadrons at intermediate p_T (2 to 5 GeV/c) [11, 12]. Deviations from such a scaling at lower beam energies could be an indication for the absence of the deconfined phase [13].

Figure 5 shows the differences in v_2 between particles X (p, Λ, Ξ^-, π^+, K^+) and corresponding anti-particles $\overline{X}$ ($\bar{p}$, $\overline{\Lambda}$, $\overline{\Xi}^+$, π^-, K^-) with $\sqrt{s_{NN}}$. Larger v_2 values are found for particles than for antiparticles, except for pions for which the opposite ordering is observed. The difference increases with decreasing beam energy and is larger for baryons compared to mesons [14].

As discussed previously, the universal NCQ scaling of v_2 at $\sqrt{s_{NN}} = 200$ GeV suggests strongly interacting partonic matter is produced. The observed difference in v_2 at lower beam energies demonstrates that this common NCQ scaling of particles and anti-particles splits. Such a breaking of the NCQ scaling could indicate increased contributions from hadronic interactions in the system evolution with decreasing beam energy, or could be related to the larger values of μ_B.
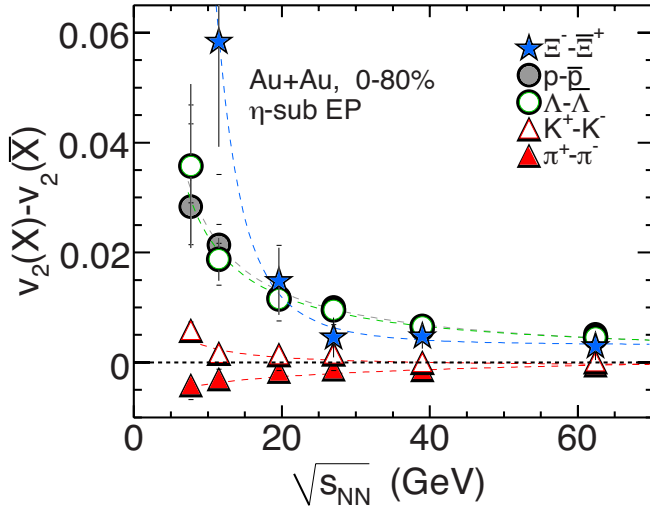
Figure 5. The difference in v_2 between particles (X) and their corresponding anti-particles ($\overline{X}$) (see legend) as a function of $\sqrt{s_{NN}}$ for 0–80% central Au+Au collisions. The dashed lines in the plot are fits with a power-law function [14].

4. Search for Critical Point

### 4.1. Particle Ratio Fluctuations

The energy dependence of particle-ratio fluctuations is also an interesting topic. Enhanced fluctuations are one of the possible signatures of a phase transition near a critical point. The observable ν_{dyn} for kaons and pions can be written as

$$\nu_{\mathrm{dyn},K\pi} = \frac{<K(K-1)>}{<K>^2} + \frac{<\pi(\pi-1)>}{<\pi>^2} - \frac{2<K\pi>}{<K><\pi>} \qquad (2)$$

Figure 6 shows the $\nu_{\mathrm{dyn},K\pi}$ results for 7.7 - 200 GeV [15, 16, 17]. STAR results are approximately independent of collision energy. This disagrees with NA49's results, which show a strong increase with decreasing incident energy. The same figure also shows model calculations. The points labeled STAR UrQMD represent UrQMD calculations with STAR acceptance cuts, which show little energy dependence and over predict the magnitude of the data. The HSD model predicts increased fluctuations at low energies and agrees with the NA49 measurements at the lowest energies but over predict the data at higher energies. None of the models presented here can fully describe the incident energy dependence of the data.

Unlike the results for K/π fluctuations, the results for p/π fluctuations are affected by resonance correlations (e.g. Δ, Λ, Σ all decay to p, π). These correlations increase the cross-correlation terms of ν_{dyn} and produce a negative ν_{dyn} value. Figure 7 shows the incident energy
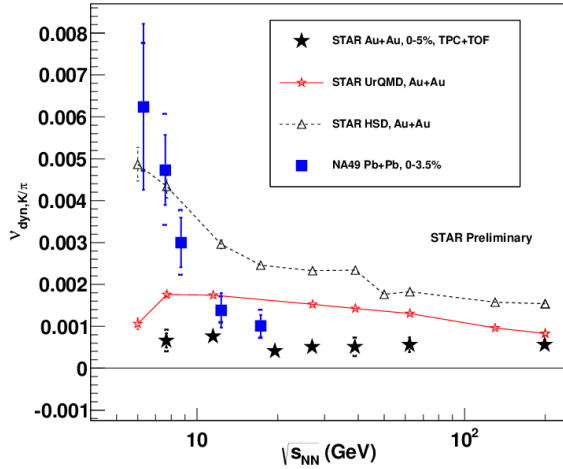
Figure 6. Energy dependence of K/π fluctuations. Only central events are shown here (0-5% for STAR Au+Au collisions,0-3.5% for NA49 Pb+Pb collisions). UrQMD and HSD calculations are also shown.
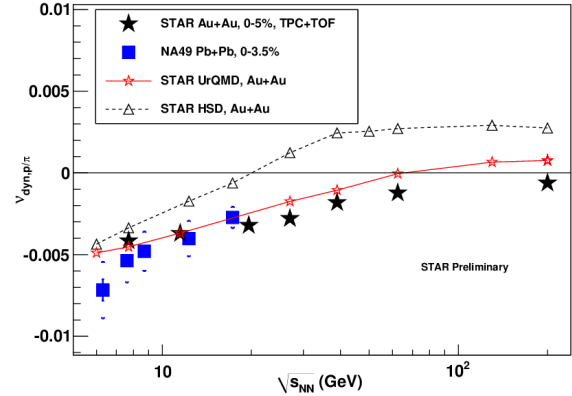
Figure 7. Energy dependence of p/π fluctuations expressed as $\nu_{\mathrm{dyn},p/\pi}$. Only central events are shown here (0-5% for STAR Au+Au collisions,0-3.5% for NA49 Pb+Pb collisions). UrQMD and HSD calculations are also shown.

dependence of $\nu_{\mathrm{dyn},p\pi}$. The STAR and NA49 results for p/π fluctuations show good agreement. They are both negative and increase with increasing collision energy. The UrQMD model describes the data well at SPS energies, which supports the resonance correlations interpretation because UrQMD is a hadronic transport model. However, UrQMD becomes positive and over predicts the data at higher energies.

p/K fluctuations, which are related to baryon-strangeness correlations, can be used as a tool to study the deconfinement phase transition. Figure 8 shows the incident energy dependence of $\nu_{\mathrm{dyn},Kp}$ results. The STAR data show a smooth decrease with decreasing collision energy and disagree with NA49 data at 7.7 GeV. Further study is still needed to understand the differences between the two experiments. A UrQMD calculation with the STAR acceptance filter is also shown in the same figure. UrQMD always over predicts fluctuations and becomes positive at high collision energies. The HSD model always predicts positive ν_{dyn} results.
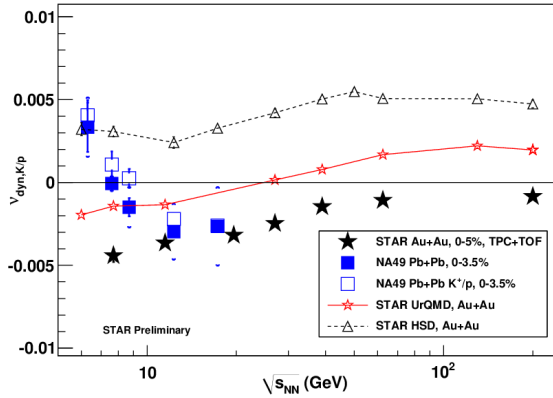
4.2. p_t Fluctuations
The p_t fluctuations could also serve as a signal for the QCD critical point or the occurrence of thermalization and collectivity [18, 19]. One observable for the event-by-event two particle momentum correlation is defined [20] as

$$\langle \Delta p_{t,i} \Delta p_{t,j} \rangle = \frac{1}{N_{\mathrm{event}}} \sum_{k=1}^{N_{\mathrm{event}}} \frac{C_k}{N_k(N_k-1)}, \tag{3}$$

where

$$C_k = \sum_{i=1}^{N_k} \sum_{j=1, i \neq j}^{N_k} \left(p_{t,i} - \langle\langle p_t \rangle\rangle \right) \left(p_{t,j} - \langle\langle p_t \rangle\rangle \right). \tag{4}$$

Figure 9 shows the incident energy dependence of p_t correlations. The STAR data shows a rapid increase from 7.7 to 62.4 GeV and then little energy dependence up to 2.76 TeV. UrQMD

Figure 8. Energy dependence of p/K fluctuations. Only central events are shown here (0-5% for STAR Au+Au collisions,0-3.5% for NA49 Pb+Pb collisions). UrQMD and HSD calculations are also shown.
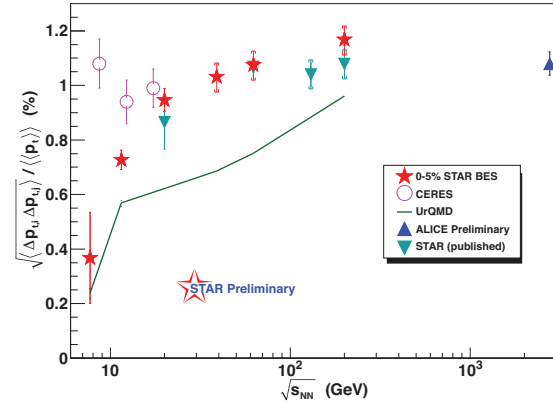

Figure 9. $\sqrt{\langle \Delta p_{t,i} \Delta p_{t,j} \rangle} / \langle \langle p_t \rangle \rangle$ as a function of incident energy. Only central events from STAR, ALICE and CERES are shown here. UrQMD calculations are also shown in the same figure.

shows a similar increasing trend but under predicts the measured correlations. The CERES data deviates from STAR at lower energy. Effects due to different experimental acceptances are still under investigation.

5. Search for First Order Phase Transition

One important goal of the STAR BES program is to search for the evidence of a first order phase transition. The HBT technique can be used to determine the freeze-out eccentricity ε_F. A non-monotonic behavior of ε_F as a function of energy could indicate a soft point in the equation of state. Figure 10 shows the excitation function of the freeze-out eccentricity. The combined E895 and STAR data shows a smooth decrease of ε_F with energy. Also, the UrQMD model reproduces both E895 and STAR data. Overall, no non-monotonic behavior is observed in ε_F.
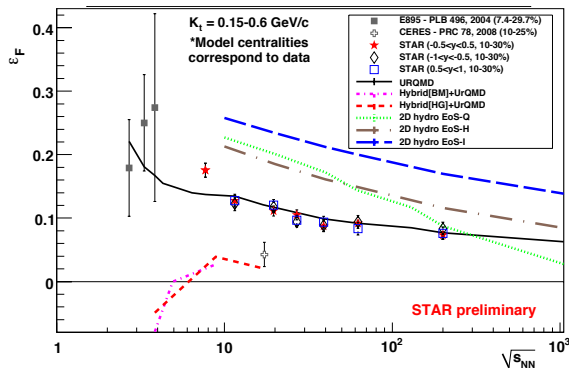
Figure 10. Freeze-out eccentricity, ϵ_F, as a function of $\sqrt{s_{NN}}$ for data and models [22].
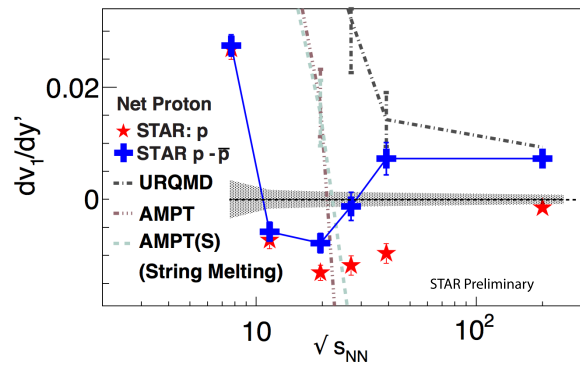
Figure 11. Directed flow slope (dv_1/dy') near mid-rapidity as a function of beam energy for mid-central(10-40%) Au+Au collisions, where the primed quantity y' refers to normalized rapidity y/y_{beam} [23].

Directed flow, which measures the "side-splash" motion of the collision products, is sensitive

Collider mode $\sqrt{s_{NN}}$ (GeV)	Fixed-target mode $\sqrt{s_{NN}}$ (GeV)	μ_B (MeV)
19.6	4.5	585
15	4.0	625
11.5	3.5	670
7.7	3.0	720
5	2.5	775

Table 1. Summary of collider mode $\sqrt{s_{NN}}$, fixed target mode $\sqrt{s_{NN}}$, and corresponding μ_B values [24].

to the equation of state (EOS) and hence can be considered a first order phase transition signal [21]. Figure 11 shows the energy dependence of directed flow slope (dv_1/dy') near mid-rapidity for 10-40% central Au+Au collisions. The v_1 slope for net protons is calculated via the relation $F = rF_{\bar{p}} + (1 - r)F_{\text{transp}}$, where r is the observed ratio of antiprotons to protons among the analyzed tracks. The net proton v_1 slope changes sign twice and shows a minimum at $\sqrt{s_{NN}} =$10 to 20 GeV. This result is qualitatively different from UrQMD and AMPT transport models, which both predict a monotonic trend throughout $\sqrt{s_{NN}} =$7.7 to 200 GeV [23]. Further studies are needed to understand the current results and their implications for the Equation of State.

6. BES Phase II
As discussed above, The BES Phase I program from STAR has some interesting results. However, there are several other observables such as higher moments of net-protons distributions and ϕ-meson v_2, which show some hints but are not statistically proficient enough to draw quantitative conclusions. To confirm these results, we need more statistics at lower energies. Another energy point at around 15 GeV is also necessary to fill the large gap in μ_B between 11.5 and 19.6 GeV. To address these problems, STAR has proposed a BES phase II program, which requests more data at these energies. With the help of electron cooling and longer bunches, we are expecting a luminosity increase of a factor of about 3-5 at 7.7 GeV and about 10 around 19.6 GeV. STAR is also planning to upgrade the inner sectors of the existing Time Projection Chamber (iTPC). This will increase the acceptance at low p_t and extend the pseudo-rapidity coverage by approximately half a unit. The increased acceptance combined with higher statistics will improve the current measurement significantly and make possible measurements of rare probes such as dilepton and hypertriton production.

In order to reach higher μ_B, STAR has also proposed to run in "fixed-target mode" by putting a gold target inside the beam pipe [25] . This will allow STAR to run at energies lower than 7.7GeV and allow the μ_B to be extended from 400MeV to 800MeV without affecting normal RHIC operation. A previous study from NA49 has reported signatures of the onset of deconfinement near $\sqrt{s_{NN}} =$7.7 GeV [26]. To confirm this, it is important to take data both below and above the transition energy. Table 1 shows a summary of collider mode, fixed target mode $\sqrt{s_{NN}}$, and corresponding μ_B values.

7. Summary
We have presented the latest results from the STAR BES Phase I program. Most results show a smooth change vs. incident energy. We do see significant differences in particle and anti-particle v_2, which indicates the breaking of the NCQ scaling. A possible minimum at $\sqrt{s_{NN}} =$10–20 GeV is also observed for the net proton v_1 slope. More statistics are needed to confirm a few other interesting observables such as higher moments of net-protons distributions and ϕ-meson v_2. We

are looking forward to the BES Phase II program with STAR iTPC upgrade and fixed-target mode.

References

[1] Y. Aoki *et al.* Nature **443**, 675-678 (2006)
[2] Shinji Ejiri, Phys. Rev. D **78** 074507 (2008)
[3] M. A. Stephanov PoS LAT2006:024,2006
[4] M.M.Aggarwal *et al.* [STAR Collaboration], arXiv:1007.2613v1
[5] J. Cleymans et al., Computer Physics Communications,180, 84 (2009).
[6] Sabita Das, [STAR Collaboration], arXiv:1210.6099
[7] A. Andronic et al., Nucl. Phys. A 834, 237 (2010).
[8] J. Cleymans et al., Phys. Rev. C 73, 034905 (2006)
[9] S.A. Bass, P. Danielewicz, and S. Pratt, Phys. Rev. Lett. **85**, 2689 (2000).
[10] B. I. Abelev *et al.* [STAR Collaboration], Phys. Rev. C **82**, 024905 (2010).
[11] J. Adams *et al.* [STAR Collaboration], Phys. Rev. Lett. **95**, 122301 (2005).
[12] B. I. Abelev *et al.* [STAR Collaboration], Phys. Rev. C **75**, 054906 (2007).
[13] M. M. Aggarwal *et al.* [STAR Collaboration], arXiv:1007.2613 [nucl-ex] (2010).
[14] L. Adamczyk *et al.* [STAR Collaboration], Phys. Rev. Lett. **110**, 142301 (2013).
[15] C. Alt et al., Phys. Rev. C **79**, 044910 (2009).
[16] J. Adams *et al.* [STAR Collaboration], Phys. Rev. Lett. **103**, 092301 (2009)
[17] Terence J Tarnowsky [STAR Collaboration], arXiv:1110.2222 [nucl-ex].
[18] M.A. Stephanov, K. Rajagopal and E.V. Shuryak Phys. Rev. Lett. **81** 4816-9 (1998).
[19] S. Gavin Phys. Rev. Lett. **92** 162301 (2004).
[20] J. Adams *et al.* [STAR Collaboration], Phys. Rev. C **72**, 044902 (2005).
[21] R. Snellings *et al.*, Phys. Rev. Lett. **84**, 2803 (2000); J. Brachmann *et al.*, Phys. Rev. C **61**, 024909 (2000);
      L. P. Csernai and D. Rohrich, Phys. Lett. B **458**, 454 (1999); H. Stoecker, Nucl. Phys. A **750**, 121 (2005).
[22] N. Shah [STAR Collaboration], arXiv:1210.5436 [nucl-ex].
[23] Yadav Pandit [STAR Collaboration], arXiv:1210.5315[nucl-ex] (2012).
[24] J. Cleymans *et al.*, Phys. Rev. C **73**, 034905 (2006).
[25] RHIC Beam Use Request For Runs 13 and 14
[26] NA49 Collaboration, Phys. Rev. C 77, 024903 (2008).